RoboPol: first season rotations of optical polarization plane in blazars

D. Blinov[1,7]⋆, V. Pavlidou[1,2], I. Papadakis[1,2], S. Kiehlmann[3], G. Panopoulou[1],
I. Liodakis[1], O. G. King[4], E. Angelakis[3], M. Baloković[4], H. Das[6], R. Feiler[5],
L. Fuhrmann[3], T. Hovatta[8], P. Khodade[6], A. Kus[5], N. Kylafis[2,1], A. Mahabal[4],
I. Myserlis[3], D. Modi[6], B. Pazderska[5], E. Pazderski[5], I. Papamastorakis[1,2],
T. J. Pearson[4], C. Rajarshi[6], A. Ramaprakash[6], P. Reig[2,1], A. C. S. Readhead[4],
K. Tassis[1,2], J. A. Zensus[3]

[1] *Department of Physics and Institute for Plasma Physics, University of Crete, GR-71003, Heraklion, Greece*
[2] *Foundation for Research and Technology - Hellas, IESL, Voutes, 7110 Heraklion, Greece*
[3] *Max-Planck-Institut für Radioastronomie, Auf dem Hügel 69, 53121 Bonn, Germany*
[4] *Cahill Center for Astronomy and Astrophysics, California Institute of Technology, 1200 E California Blvd, MC 249-17,*
Pasadena CA, 91125, USA
[5] *Toruń Centre for Astronomy, Nicolaus Copernicus University, Faculty of Physics, Astronomy and Informatics,*
Grudziadzka 5, 87-100 Toruń, Poland
[6] *Inter-University Centre for Astronomy and Astrophysics, Post Bag 4, Ganeshkhind, Pune - 411 007, India*
[7] *Astronomical Institute, St. Petersburg State University, Universitetsky pr. 28, Petrodvoretz, 198504 St. Petersburg, Russia*
[8] *Aalto University Metsähovi Radio Observatory, Metsähovintie 114, FL-02540 Kylmälä, Finland*

ABSTRACT

We present first results on polarization swings in optical emission of blazars obtained by RoboPol, a monitoring programme of an unbiased sample of gamma-ray bright blazars specially designed for effective detection of such events. A possible connection of polarization swing events with periods of high activity in gamma rays is investigated using the data set obtained during the first season of operation. It was found that the brightest gamma-ray flares tend to be located closer in time to rotation events, which may be an indication of two separate mechanisms responsible for the rotations. Blazars with detected rotations during non-rotating periods have significantly larger amplitude and faster variations of polarization angle than blazars without rotations. Our simulations show that the full set of observed rotations is not a likely outcome (probability $\leq 1.5 \times 10^{-2}$) of a random walk of the polarization vector simulated by a multicell model. Furthermore, it is highly unlikely ($\sim 5 \times 10^{-5}$) that none of our rotations is physically connected with an increase in gamma-ray activity.

Key words: polarization – galaxies: active – galaxies: jets – galaxies: nuclei

1 INTRODUCTION

Blazars are active galactic nuclei whose jets are oriented close to our line of sight, so that we observe high relativistic beaming of their non-thermal emission and large amplitude variability at all wavelengths. The low-frequency emission is dominated by synchrotron radiation, and hence is highly polarized. The exact polarization fraction and direction depend on the structure of the magnetic field in the emitting region, and on the number of emitting re-

gions along the line of sight. The polarization direction (in the simple case of a single dominant emission region) traces (and is perpendicular to) the direction of the projected magnetic field on the plane of the sky. Already from early optical observations, it has been known that polarization parameters of blazars are variable on daily time-scales (Kinman et al. 1966). In general, both flux density and polarization exhibit an erratic variability (Angel & Stockman 1980; Uemura et al. 2010; Ikejiri et al. 2011), which could be interpreted as a random walk (Moore et al. 1982). However, in some cases the electric vector position angle (EVPA) of the polarized emission displays long, smooth and mono-

⋆ E-mail: blinov@physics.uoc.gr

Table 1. Selection criteria for the gamma-ray–loud and the control sample.

Property	Gamma-ray–loud sample	Control sample
2FGL	included	not included
2FGL F(E > 100 MeV)	$> 10^{-8}\,\mathrm{cm}^{-2}\,\mathrm{s}^{-1}$	–
2FGL source class	agu, bzb, or bzq	–
Galactic latitude $\|b\|$	$> 10°$	–
Elevation (Elv) constraints[1]	$\mathrm{Elv_{max}} \geq 40°$ for at least 90 consecutive nights in the window June – November	$\mathrm{Elv_{max}} \geq 40°$ for at least 90 consecutive nights in the window April – November
R magnitude[2]	≤ 17.5	≤ 17.5
CGRaBS/15 GHz OVRO monitoring	no constraints	included
OVRO 15 GHz mean flux density	no constraints	$\geq 0.060\,\mathrm{Jy}$
OVRO 15 GHz intrinsic modulation index, m	no constraints	≥ 0.05

[1] Refers to elevation during Skinakas dark hours
[2] Average value between archival value and measured during preliminary RoboPol observations (when applicable)

tonic rotations which have been observed in the optical since the 1980s (Kikuchi et al. 1988). A number of mechanisms have been proposed for the interpretation of such events, including: stochastic variations of turbulent magnetic fields, a shock travelling through a non-axisymmetric magnetic field (Konigl & Choudhuri 1985), polarized flares in the accretion disc (Sillanpää et al. 1993), two-component models consisting of two independent sources of polarized emission (Bjornsson 1982), and jet bending (Abdo et al. 2010a).

Blazars represent the most common class of known gamma-ray sources (Nolan et al. 2012; Acero et al. 2015). Despite the recent progress in the field, many questions concerning the high-energy emission produced by blazars are still under debate. For instance, it is unclear where the gamma-ray emitting site is located: within the broad-line region (e.g. Blandford & Levinson 1995; Poutanen & Stern 2010) or well downstream in the jet (e.g. Marscher et al. 2008; Agudo et al. 2011).

Recent work showed that at least some large EVPA swings can be associated with gamma-ray flares (e.g. Abdo et al. 2010a; Larionov et al. 2013b) and therefore can possibly provide some insight on the physics of high-energy activity. Although such events have triggered an increasing interest in polarimetric monitoring of gamma-ray blazars, efforts in this direction have been based on selected cases comprising statistically biased samples. As a result, a significant amount of invaluable polarimetric data sets for a large number of sources has been gathered. However, this set cannot be used for statistically rigorous population studies and, in particular, the investigation of a possible correlation between gamma-ray flares and optical EVPA rotations. The RoboPol programme (King et al. 2014; Pavlidou et al. 2014) has been designed to provide a data set of rotation events in an unbiased sample of blazars, appropriate for such studies.

In this paper, we analyse EVPA rotations detected by RoboPol during the first observing season between 2013 July and November. After a brief description of observing and reduction techniques in Sec. 2, we estimate the frequency of

EVPA rotations in blazars and list their properties in Sec. 3. A Monte Carlo simulation is performed in Sec. 4 in order to determine whether the EVPA rotations can be produced by random walk processes. In Sec. 5 we study the possible connection between an increased activity in the gamma-ray band and EVPA swings. Our findings are summarized in Sec. 6.

## 2 OBSERVATIONS AND DATA REDUCTION

2.1 Our sample

A unique feature of the RoboPol programme is that it is monitoring a sample which has been selected on the basis of strict, bias-free and objective criteria (for detailed discussion on the sample construction, see Pavlidou et al. 2014). The sample consists of three distinct groups.

(i) The main ("gamma-ray–loud") sample is an unbiased subset of a statistically complete flux-limited sample of blazars from the second *Fermi*-LAT source catalogue (Nolan et al. 2012). Specifically, we selected all the sources in the 2FGL catalogue classified as BL Lacertae objects (bzb), Flat Spectrum Radio Quasars (bzq), or active galaxy of uncertain type (agu). Applying the selection criteria listed in Table 1, we constructed a gamma-ray flux-limited "parent sample". Application of the visibility constraints and field-quality cuts resulted in an unbiased subsample of 83 sources, among which we randomly selected 62 sources.

(ii) A "control" sample of 15 "gamma-ray–quiet" sources. It constitutes an unbiased subset of a statistically complete sample of blazars. It has been drawn from the CGRaBS catalogue (Healey et al. 2008) applying the selection criteria listed in Table 1.

(iii) 24 additional sources chosen on the basis of their variability characteristics or their presence either in the F-GAMMA programme sample or in TeV catalogues.
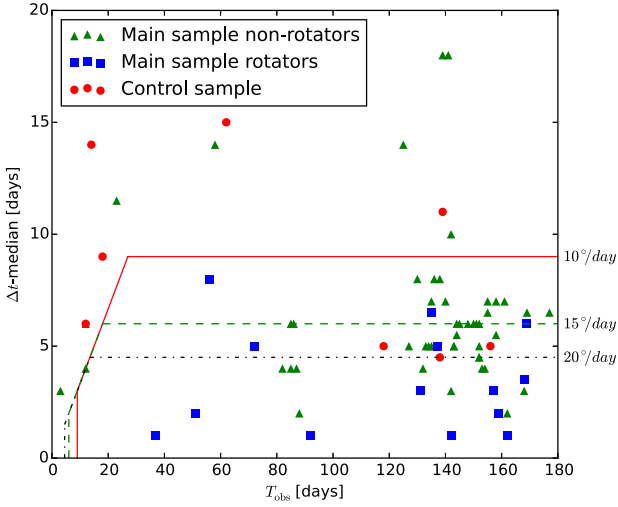
Figure 1. Season length and median cadence for the first season data. Broken lines limit areas where rotations at rates of 10, 15 and 20 deg d^{-1} can be detected (see Sec. 3.3 for details). Only objects with Δt-median ≤ 20 were left for the more detailed view.

Although here we present the polarization swings detected in all monitored sources during the first RoboPol observing season, the statistical analysis in this paper is based only on sources from the group (i).

2.2 Optical observations

All photometric and polarimetric measurements were done at the 1.3-m telescope of Skinakas observatory[1] using RoboPol, a polarimeter specifically built for the project (King et al. 2014). The RoboPol instrument contains a fixed set of two Wollaston prisms and half-wave plates, which splits each incident ray into four rays with polarization plane rotated 45° with respect to each other. Measuring relative intensities in pairs of the rays for each object in the 13 arcmin × 13 arcmin field, we obtain the fractional Stokes parameters $q = (I_1 - I_2)/(I_1 + I_2) = Q/I$ and $u = (I_3 - I_4)/(I_3 + I_4) = U/I$. Stokes parameter I is calculated as a sum of intensities of all four spots. Since the polarization parameters are measured simultaneously, we avoid unmeasurable errors caused by the sky changes between measurements and imperfect alignment of rotating optical elements.

The data presented in this paper were taken with the R-band filter. Magnitudes were calculated using calibrated field stars either found in the literature or presented in PTF (Palomar Transient Factory) R-band catalogue (Ofek et al. 2012) or USNO-B1.0 catalogue (Monet et al. 2003), depending on availability.

The exposure length was adjusted by the brightness of each target, which was estimated during the short pointing exposures, depending also on the sky conditions. The average photometric error in magnitudes is 0.04 mag. The data were processed using the specialized pipeline described in

detail by King et al. (2014) along with the telescope control system.

Since we have introduced a Galactic latitude cut selecting objects with $|b| > 10°$, the average colour excess in the directions of our targets is relatively low, $\overline{E(B-V)} = 0.11^m$ (Schlafly & Finkbeiner 2011), implying that the interstellar polarization is less than 1.0% on average (Serkowski et al. 1975). The statistical uncertainty in the degree of polarization is less than 1% in most cases, while the EVPA is typically determined with a precision of $1° - 10°$ depending on the source brightness and fractional polarization. Detailed description of the instrument model and error analysis is given in King et al. (2014).

In order to resolve the 180° ambiguity of the EVPA we followed a standard procedure (see e.g. Abdo et al. 2010a; Ikejiri et al. 2011; Kiehlmann et al. 2013), which is based on the assumption that temporal variations of the EVPA are smooth and gradual, hence adopting minimal changes of the EVPA between consecutive measurements. We define the EVPA variation as $\Delta\theta_n = |\theta_{n+1} - \theta_n| - \sqrt{\sigma(\theta_{n+1})^2 + \sigma(\theta_n)^2}$, where θ_{n+1} and θ_n are the $n+1$ and n-th points of the EVPA curve and $\sigma(\theta_{n+1})$ and $\sigma(\theta_n)$ are the corresponding errors of the position angles. If $\Delta\theta_n > 90°$, we shift the angle θ_{n+1} by $\pm n \times 180°$, where the integer $\pm n$ is chosen in such a way that it minimizes $\Delta\theta_n$. If $\Delta\theta_n \leq 90°$, we leave θ_{n+1} unchanged.

Our first period of regular photometric and polarimetric monitoring of blazars started in 2013 July and lasted until the end of 2013 November. During the five-month period we obtained more than 1100 measurements of 101 objects from our sample almost uniformly spread over the observing season of each object. The median cadence and total season length for objects with Δt-median smaller than 20 d (including the June survey data, Pavlidou et al. 2014) is presented in Fig. 1, which is discussed in more detail in Sec. 3.3.

2.3 Gamma-ray observations

The gamma-ray data were obtained with the Large Area Telescope (LAT) onboard the *Fermi* gamma-ray space observatory, which observes the entire sky every 3 h at energies of 20 MeV – 300 GeV (Atwood et al. 2009). We analysed LAT data in the energy range 100 MeV $\leq E \leq$ 100 GeV using the unbinned likelihood analysis of the standard *Fermi* analysis software package Science Tools v9r33p0 and the instrument response function $P7REP\_SOURCE\_V15$. Source class photons (evclass=2) were selected within a 15° region of interest centred on a blazar. Cuts on the satellite zenith angle ($< 100°$) and rocking angle ($< 52°$) were used to exclude the Earth limb background. The diffuse emission from the Galaxy was modelled using the spatial model $gll\_iem\_v05\_rev1$. The extragalactic diffuse and residual instrumental backgrounds were included in the fit as an isotropic spectral template iso_source_v05. The background models[2] include all sources from the 2FGL catalogue within 15° of the blazar. Photon fluxes of sources beyond 10° from the blazar and spectral shapes of all targets were fixed to their values reported in 2FGL. The source is considered to

Table 2. Observational data for EVPA rotations detected by RoboPol in 2013. Columns (1),(2) - blazar identifiers; (3) - redshift; (4) - observational season length; (5) - average rotation rate; (6) - total amplitude of EVPA change; (7) - number of observations during rotation; (8) - time duration of the rotation; (9) - TeV emission flag according to TeVCat[14] ("Y" means that the blazar has been detected in gamma rays with $E > 1$ TeV, "N" - otherwise); (10) - blazar subclass (LBL, IBL, HBL denote low, intermediate and high synchrotron peaked BL Lacertae objects, FSRQ – flat spectrum radio quasar).

Blazar ID	Survey name	z	T_{obs} (d)	$\langle\frac{\Delta\theta}{\Delta t}\rangle$ (deg/d)	$\Delta\theta_{max}$ (deg)	N_{points}	T_{rot} (d)	TeV	Class
RBPLJ0136+4751	OC 457	0.859[1]	59	-6.6	-225	6	34	N	FSRQ[13]
RBPLJ0259+0747	PKS0256+075	0.893[2]	72	-4.8	-180	6	38	N	FSRQ[13]
RBPLJ0721+7120*	S5 0716+71	0.31[3]	88	-14.8	-208	11	14	Y	LBL[10]
RBPLJ0854+2006*	OJ 287	0.306[4]	51	-6.7	-154	10	23	N	LBL[10]
RBPLJ1048+7143	S5 1044+71	1.15[5]	142	-9.0	-188	22	21	N	–
RBPLJ1555+1111	PG 1553+113	–	129	5.6	128	8	23	Y	HBL[10]
RBPLJ1558+5625	TXS1557+565	0.3[6]	137	7.2	222	9	31	N	IBL?[11]
RBPLJ1806+6949	3C 371	0.05[7]	143	-16.5	-347	7	21	N	LBL[11]
RBPLJ1806+6949	–//–	–//–	–//–	13.3	238	5	18	N	–//–
RBPLJ1927+6117	S4 1926+61	–	135	-4.4	-105	6	24	N	LBL[13]
RBPLJ2202+4216	BL Lac	0.069[8]	137	-51.0	-253	5	5	Y	LBL[10]
RBPLJ2232+1143	CTA 102	1.037[1]	140	-15.6	-312	8	20	N	FSRQ[13]
RBPLJ2232+1143	–//–	–//–	–//–	-11.8	-140	6	12	N	–//–
RBPLJ2243+2021	RGB J2243+203	–	169	-5.9	-183	5	31	N	LBL[12]
RBPLJ2253+1608	3C 454.3	0.859[1]	159	-18.3	-129	4	7	N	FSRQ[13]
RBPLJ2311+3425	B2 2308+34	1.817[9]	36	3.3	74	20	23	N	FSRQ[13]

* Source belongs to sample (iii)

[1](Hewitt & Burbidge 1987);[2](Murphy et al. 1993);[3](Nilsson et al. 2008);[4](Nilsson et al. 2010);
[5](Polatidis et al. 1995);[6](Falco et al. 1998);[7](de Grijp et al. 1992);[8](Vermeulen et al. 1995);
[9](Wills & Wills 1976);[10] (Donato et al. 2001);[11](Ghisellini et al. 2011);[12](Nieppola et al. 2006);
[13](Fan et al. 2012);[14]http://tevcat.uchicago.edu

be detected if the test statistic, TS, provided by the analysis exceeds 10, which corresponds to approximately a 3σ detection level (Nolan et al. 2012). The systematic uncertainties in the effective LAT area do not exceed 10 per cent in the energy range we use (Ackermann et al. 2012). This makes them insignificant with respect to the statistical errors, that dominate over the short time-scales analysed in this paper. Moreover our analysis is based on the relative flux variations. Therefore the systematic uncertainties were not taken into account.

Different time bins t_{int}, from 1 week to 25 d were used, depending on the flux density of the object. In order to make the analysis more robust we increased sampling of the photon flux curves shifting centres of the time bins by $t_{int}/4$ interval from each other. This prevents losses of possible short-term events in the light curves and reduces the dependence of results on the particular position of the time bins. The oversampling introduces an autocorrelation in the photon flux curves, which is however inessential for the analysis used in this work.

3   RESULTS
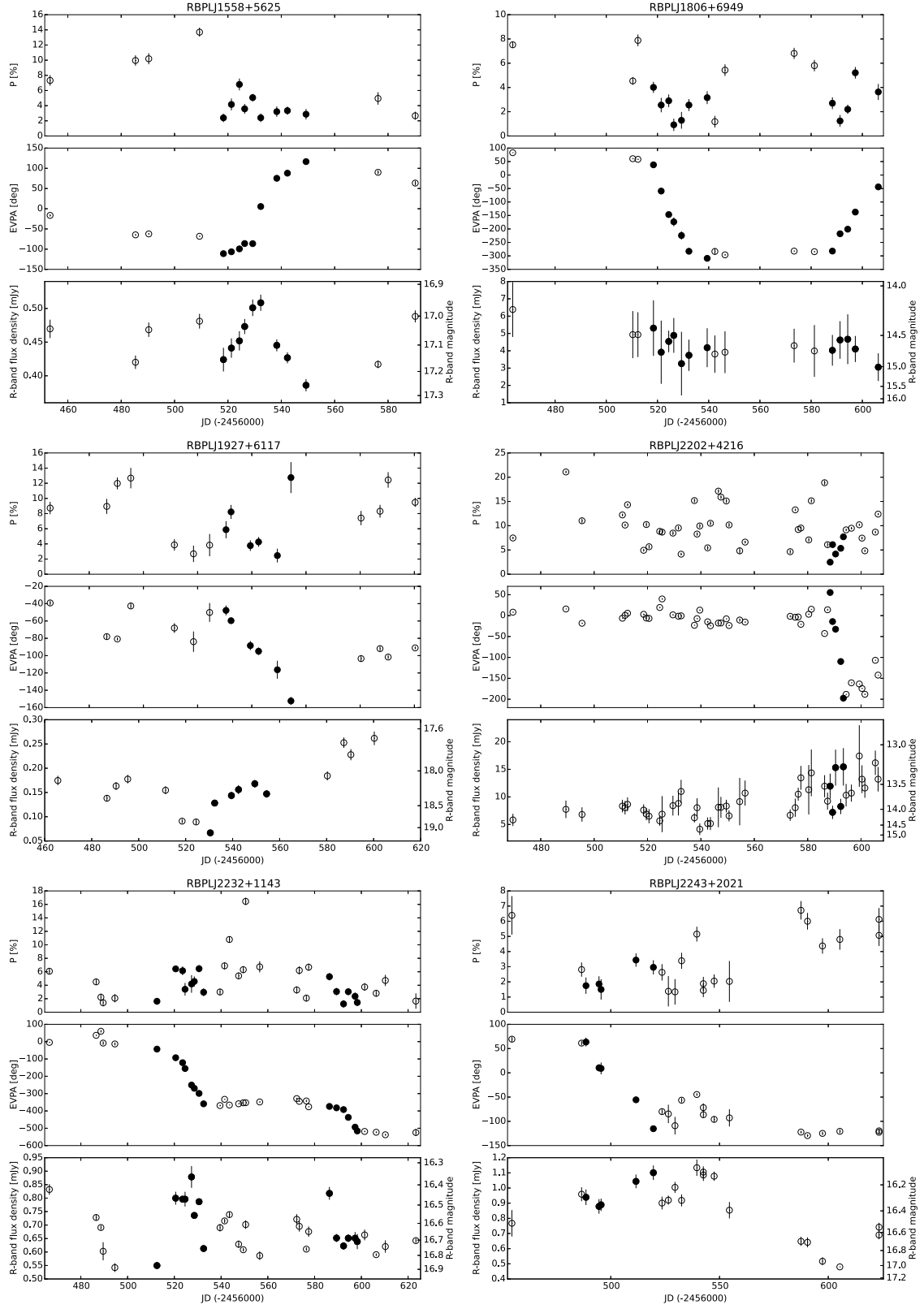
3.1   Detected rotations of EVPA

The optical emission polarization plane of blazars is often variable even within the course of a single night. There is no objective physical definition of an EVPA rotation. Strictly speaking, any change of the EVPA between two measurements constitutes a rotation. However typically only high-amplitude ($> 90°$), smooth and well tracked variations of the EVPA are considered as rotations in the literature.

We accept a swing between two consecutive EVPA measurements $\Delta\theta = |\theta_{i+1} - \theta_i|$ as significant if $\Delta\theta > \sqrt{\sigma(\theta_{i+1})^2 + \sigma(\theta_i)^2}$. We define as an EVPA rotation any continuous change of the EVPA curve with a total amplitude $\Delta\theta_{max} > 90°$, which is comprised by at least four measurements with significant swings between them. Start and end points of a rotation event are defined by a change of the EVPA curve slope $\Delta\theta_i/\Delta t_i$ by a factor of 5 or a change of its sign. This definition is rather conservative, and is in general consistent with rotations reported in the literature.

Using this definition, we identified 14 rotations of the EVPA in 12 blazars from the main sample during the season of 2013 (see Table 2). This number is comparable to the number of previously known events of this type. Two more blazars with detected rotations, namely RBPLJ0721+7120 and RBPLJ0854+2006, belong to the additional sample of hand-picked sources. These blazars/events were not included in the statistical or frequency analysis of the following sections in this paper. The full season EVPA curves along with the evolution of the polarization degree and the R-band flux density, for all 14 blazars with detected rotations, are shown in Fig. 2 and listed in Table 2. The EVPA rotations are marked by filled black points. Clearly the events we have considered as rotations based on our criteria are the largest $\Delta\theta_{max}$ rotation events that appear in these data sets. They are all characterized by smooth variations with a well-defined trend. Two events plotted in Fig. 2 do not follow the definition strictly. These are the rotation events detected in the data sets of RBPLJ1048+7143 and RBPLJ2311+3425. In both cases the rotations were interrupted by short, low amplitude, albeit significant swings in the opposite direction with respect to the overall rotation. Since both events are
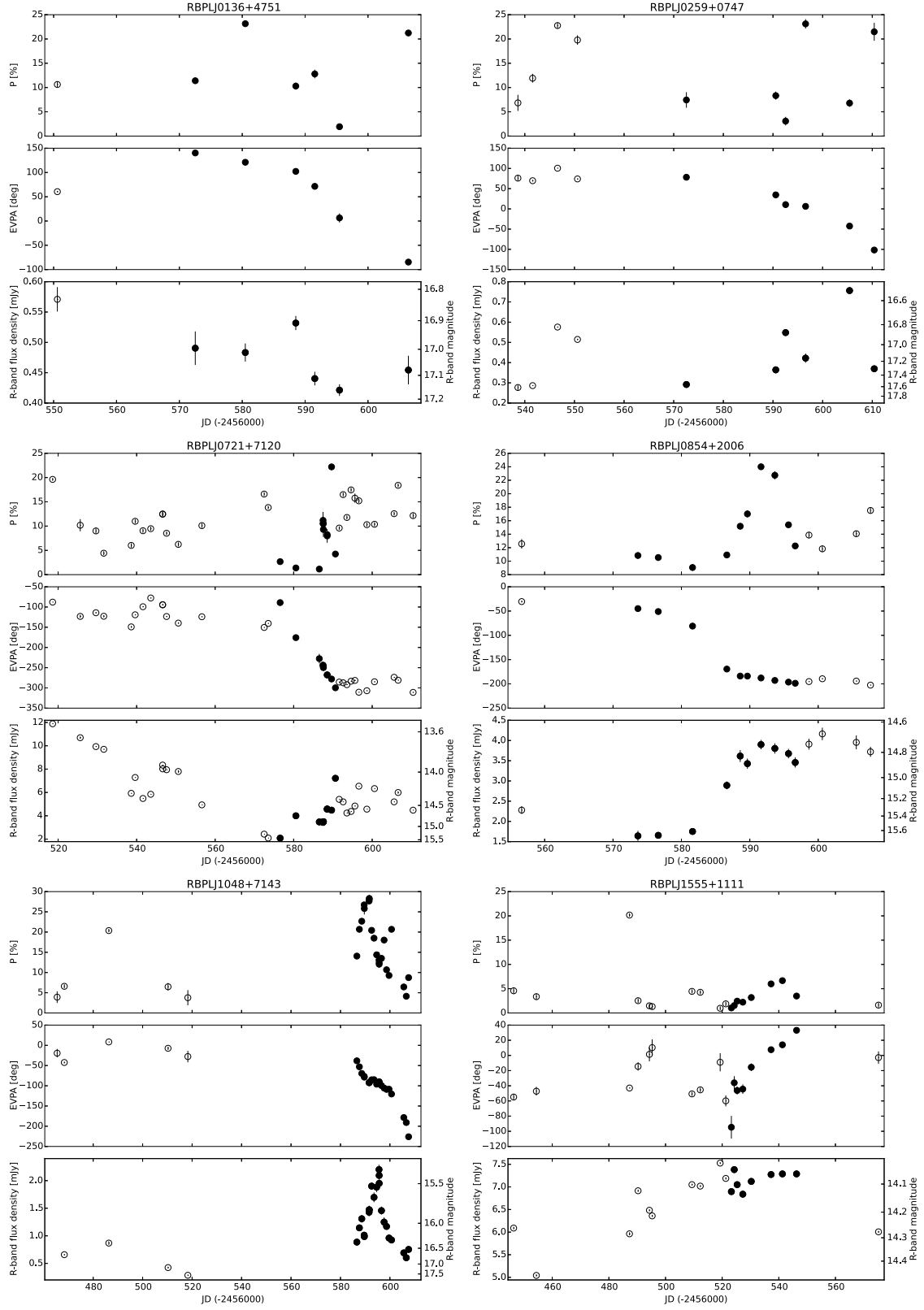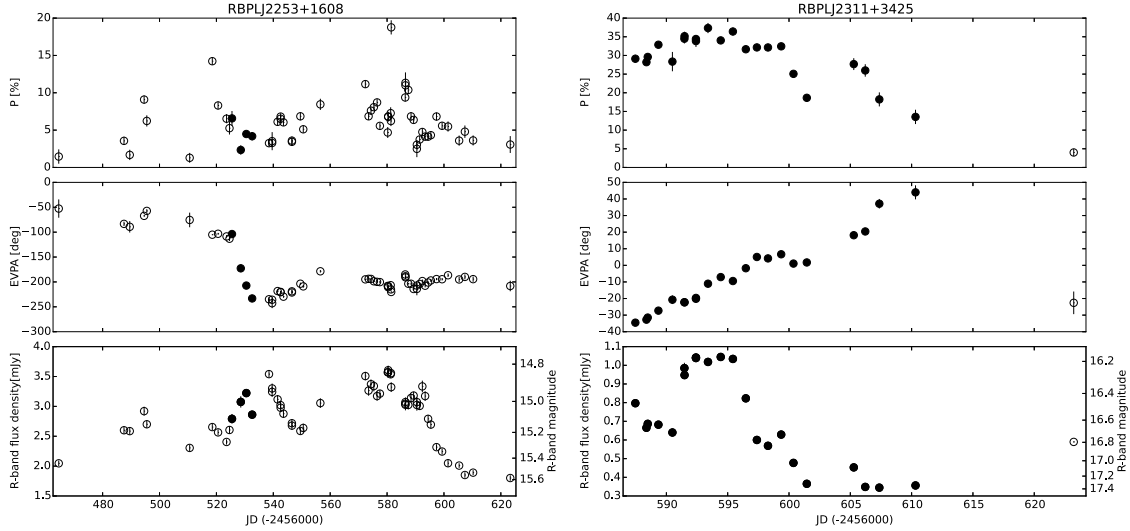
Figure 2. Evolution of polarization degree, polarization position angle and *R*-band magnitude for blazars with a detected rotation in the first RoboPol season. Periods of rotations are marked by filled black points.

Figure 2 – *continued* (Continued) Evolution of polarization degree, polarization position angle and *R*-band magnitude for blazars with a detected rotation in the first RoboPol season. Periods of rotations are marked by filled black points.

Figure 2 – *continued* (Continued) Evolution of polarization degree, polarization position angle and *R*-band magnitude for blazars with a detected rotation in the first RoboPol season. Periods of rotations are marked by filled black points.

well sampled these small deviations do not introduce any significant difference in the overall EVPA trend. Hence both events can be considered as single, large $\Delta\theta_{max}$ rotations. In addition the RBPLJ2311+3425 event has an amplitude of $\sim 74°$, which is less than the lower limit we accepted. However the start and end points of the rotation are not defined due to a sparse sampling. It is likely that this well defined EVPA change would meet the $90°$ limit if we had a longer data set for this object. It is for this reason that we include this event in our sample of rotations. Both events have not been used in any of our statistical analyses involving comparison between simulated and observed rotations.

Some of the EVPA rotation events are coincident with an increase in the total flux, as it follows from a visual inspection of Fig. 2. A quantitative comparison between the optical flux and the polarization variations will be presented in a forthcoming paper.

3.2 General properties of EVPA rotations and rotators

We estimated the maximal amplitude $\Delta\theta_{max}$ and the duration of the rotations T_{rot}, using the first and last points of each event. Due to a moderate sampling and $180°$ EVPA ambiguity, the rotation start and/or end points cannot be pinpointed accurately in five cases (namely RBPLJ0136+4761, RBPLJ0259+0747, RBPLJ1048+7143, RBPLJ1806+6949 and RBPLJ2311+3425). This ambiguity affects the estimated $\Delta\theta_{max}$ and T_{rot} of the event, which should really be considered as lower limits in this case. We also estimated the average rotation rate as $\langle\Delta\theta/\Delta t\rangle = \Delta\theta_{max}/T_{rot}$. These parameters as well as the blazar class and the TeV emission flag are listed in Table 2.

We also collected data from the literature on previously known rotations of EVPA in blazars which show this behaviour ("rotators" hereafter). Rates and $\Delta\theta_{max}$ of these rotations were estimated from plots in the respective papers. These parameters as well as the blazar class and the TeV emission flag are listed in Table 3.
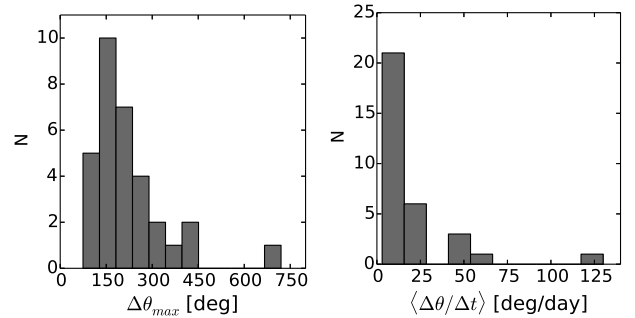
Figure 3. Distributions of amplitudes and rates of EVPA rotations detected in RoboPol's first season and reported in the literature.

The distribution of $\Delta\theta_{max}$ and rates of EVPA rotations from historical and RoboPol data are shown in Fig. 3. The number of detected rotations clearly decreases with growing $\Delta\theta_{max}$. At the same time slow rotations dominate in the sample. This is presumably caused by a selection effect, because fast rotations require better sampling of observations.

Summarizing data on all known EVPA rotations in blazars to date we can list the following properties:

(i) all known blazars with detected EVPA rotations are in the 2FGL catalogue (i.e. they are "gamma-ray–loud" sources);

(ii) there are blazars known as TeV emitters as well as non-TeV sources among rotators;

(iii) all subclasses of blazars show rotations of the EVPA, regardless of the position of the synchrotron peak maximum or the BL Lac/FSRQ dichotomy;

(iv) there are eight blazars with more than one rotation detected. Comparison of these rotations shows that a single source can show rotations in both directions (five blazars known so far with this behaviour) and rotations observed in the same source can be of significantly different rates

Table 3. Data on known rotation of optical EVPA in blazars. Columns (1),(2) - blazar identifiers; (3) - average rotation rate; (4) - total amplitude of EVPA change; (5) - TeV emission flag according to TeVCat[5] ("Y" means that the blazar has been detected in gamma rays with $E > 1$ TeV, "N" - otherwise); (6) - blazar subclass (LBL, IBL, HBL denote low, intermediate and high synchrotron peaked BL Lacertae objects, FSRQ – flat spectrum radio quasar); (7) - reference.

Blazar ID	Survey name	$\langle \frac{\Delta\theta}{\Delta t} \rangle$ (deg d^{-1})	$\Delta\theta_{max}$ (deg)	TeV	Class	Reference
RBPLJ0423−0120	PKS 0420−014	−11.1	−110	N	FSRQ[4]	(D'Arcangelo et al. 2007)
RBPLJ0721+7120	S5 0716+71	+130	+180	Y	LBL[1]	(Larionov et al. 2013b)
RBPLJ0854+2006	OJ 287	−17	−180	N	LBL[1]	(Kikuchi et al. 1988)
RBPLJ0958+6533	S4 0954+65	+18.2	+240	N	LBL[2]	(Larionov et al. 2011)
RBPLJ1221+2813	W Comae	≥ +3.0	+110	Y	IBL[3]	(Benítez et al. 2013)
RBPLJ1256−0547	3C 279	−9	−180	Y	FSRQ[4]	(Abdo et al. 2010a)
RBPLJ1256−0547	3C 279	+4.3	+290	−//−	−//−	(Larionov et al. 2008)
RBPLJ1256−0547	3C 279	+4.7	+140	−//−	−//−	(Aleksić et al. 2014a)
RBPLJ1512−0905	PKS 1510−089	+15.6	+720	Y	FSRQ[4]	(Marscher et al. 2010)
RBPLJ1512−0905	PKS 1510−089	+12	+400	−//−	−//−	(Aleksić et al. 2014b)
RBPLJ1512−0905	PKS 1510−089	−50	−250	−//−	−//−	(Aleksić et al. 2014b)
RBPLJ1512−0905	PKS 1510−089	+11.7	+500	−//−	−//−	(Sasada et al. 2011)[6]
RBPLJ2202+4216	BL Lac	+46	+220	Y	IBL[1]	(Marscher et al. 2008)
RBPLJ2202+4216	BL Lac	+21	+210	−//−	−//−	(Sillanpää et al. 1993)
RBPLJ2232+1143	CTA 102	−60	−180	N	FSRQ[4]	(Larionov et al. 2013a)
RBPLJ2253+1608	3C 454.3	+16.3	+130	N	FSRQ[4]	(Sasada et al. 2010)
RBPLJ2253+1608	3C 454.3	+9.3	+400	−//−	−//−	(Sasada et al. 2012)

[1](Donato et al. 2001);[2](Ghisellini et al. 2011);[3](Tagliaferri et al. 2000);[4](Fan et al. 2012)
[5]http://tevcat.uchicago.edu;[6]same as in Marscher et al. (2010).

(in seven blazars rates differ by a factor larger than two in speed).

3.3 Observed frequency of EVPA rotations

The efficiency of an EVPA rotation detection depends on the intrinsic rate of the rotation as well as the frequency and uniformity of the observing cadence. The ambiguity of the polarization position angle introduces an upper limit on the rotation rate that can be unequivocally detected with a given typical cadence of observations. Clearly, for a typical time interval between observations $\langle \Delta t \rangle$, no EVPA rotation with a rate higher than $90°/\langle \Delta t \rangle$ can be observed.

For each blazar in our sample we found the median time difference between successive observations Δt-median and the total observing season length (defined as the time difference between the first and the last observations) T_{obs}. These quantities (for blazars observed with Δt-median ≤ 20 days) are shown in Fig. 1. In the same figure, we also plot three lines which indicate the necessary Δt-median and T_{obs} for detection of EVPA rotations at rates ≤ 10 (solid line), ≤ 15 (dashed line) and ≤ 20 (dotted line) degrees per day.

The leftmost vertical part of each line represents the shortest T_{obs} needed to detect a rotation of $\Delta\theta_{max} = 90°$ at a given rotation rate. The inclined portion of each line is determined by our requirement on a rotation event to be comprised by a minimum of four points. Given this requirement, as Δt-median increases, so does T_{obs}. An EVPA data set with Δt-median and T_{obs} on that line can allow detection of EVPA rotations with $90° ≤ \Delta\theta_{max} ≤ 270°$. The horizontal part indicates the maximum Δt-median allowed the detection of a rotation event under the requirement of $\Delta\theta ≤ 90°$ in EVPA between two consecutive points.

We can now estimate the frequency with which EVPA

rotations appear in blazars as follows. Out of the 14 detected rotations in blazars of the main sample, 8 have rates less than 10 deg d^{-1}. There are also 41 main sample ("gamma-ray bright") blazars that were observed with Δt-median and T_{obs} (see Table 4) within the region defined by the solid line in Fig. 1. The total observing length for these blazars is 6432 d. Thereby we estimate the frequency of "slow" rotations (rate < 10 deg d^{-1}) in the main sample sources as one rotation in ∼ 800 days (6432 d / 8 rotations). Following the same reasoning we estimate average frequencies of rotations for blazars in the main sample with rates < 15 deg d^{-1} and < 20 deg d^{-1} as one rotation in ∼ 490 d (4912/10) and ∼ 180 d (2363/13), respectively.

3.4 EVPA variability in blazars of different samples

In order to address the question whether "the EVPA variability is different in objects where rotations were detected compared to the rest of the main sample and to the control sample" we collate all EVPA "swing" events and measure their $\Delta\theta_{max}$ and rates. We define an EVPA "swing" as any continuous change of the EVPA curve, without a lower limit in its $\Delta\theta_{max}$ or in the number of measurements. As before, start and end points of a swing event are defined by a change of the EVPA curve slope by a factor of 5 or a change of its sign.

We identified all such events for all blazars of the main and control samples within the 10 deg d^{-1} "detection box" in Fig. 1, and measured their amplitude, $\Delta\theta_{max}$, and mean rotation rate. The cumulative distribution function (hereafter CDF; e.g. Wall & Jenkins 2012) of the EVPA swings $\Delta\theta_{max}$ and rotation rates for blazars in the main sample which showed rotations ("rotators"), blazars in the main sample,

Table 4. Sources of the main and control samples within the $\langle\frac{\Delta\theta}{\Delta t}\rangle < 10$ deg d^{-1} "detection box".

Blazar ID (RBPL...)	Survey name	T_{obs} (d)	$\langle\Delta t\rangle$ (d)	Blazar ID (RBPL...)	Survey name	T_{obs} (d)	$\langle\Delta t\rangle$ (d)
	Main sample			J1838+4802	GB6 J1838+4802	121	7.0
J0045+2127	GB6 J0045+2127	33	4.0	J1841+3218	RXJ1841.7+3218	152	6.0
J0114+1325	GB6 J0114+1325	38	6.0	J1903+5540	TXS 1902+556	135	5.0
J0211+1051	MG1 J021114+1051	85	4.0	J1959+6508	1ES 1959+650	143	5.0
J0217+0837	ZS0214+083	85	6.0	J2005+7752	S5 2007+77	140	7.0
J0423−0120	PKS 0420−01	12	4.0	J2015−0137	PKS2012−017	155	6.5
J0841+7053	4C 71.07	71	6.0	J2016−0903	PMNJ2016−0903	155	7.0
J1512−0905	PKS 1510−08	88	2.0	J2022+7611	S5 2023+760	158	7.0
J1542+6129	GB6 J1542+6129	87	4.0	J2030−0622	TXS 2027−065	143	5.0
J1553+1256	PKS 1551+130	132	4.0	J2039−1046	TXS 2036−109	144	5.5
J1604+5714	GB6 J1604+5714	135	7.0	J2131−0915	RBS1752	127	5.0
J1607+1551	4C 15.54	136	8.0	J2143+1743	OX 169	119	5.0
J1635+3808	4C 38.41	121	2.0	J2148+0657	4C 6.69	152	4.5
J1642+3948	3C 345	148	6.0	J2149+0322	PKSB 2147+031	169	6.5
J1653+3945	Mkn 501	153	4.0	J2150−1410	TXS 2147−144	130	8.0
J1725+1152	1H 1720+117	120	3.0	J2225−0457	3C 446	144	6.0
J1748+7005	S4 1749+70	87	3.0	J2251+4030	MG4 J225201+4030	177	6.5
J1751+0939	OT 081	154	4.0	J2334+0736	TXS 2331+073	138	8.0
J1754+3212	RXJ1754.1+3212	134	5.0	J2340+8015	BZBJ2340+8015	113	5.5
J1800+7828	S5 1803+784	133	5.0		Control sample		
J1809+2041	RXJ1809.3+2041	152	4.5	J1551+5806	SBS1550+582	118	5.0
J1813+3144	B2 1811+31	150	6.0	J1638+5720	S4 1637+57	138	4.5
J1836+3136	RXJ1836.2+3136	151	6.0	J2042+7508	4C +74.26	99	5.0

which did not show rotations ("non-rotators"), as well as for blazars in the control sample, are shown in Fig. 4.

We performed a two sample Kolmogorov–Smirnov (K–S) test (e.g. Wall & Jenkins 2012) pairwise for three samples of collected swing amplitudes and rates with the null-hypothesis that these samples are drawn from the same distribution. The null-hypothesis is rejected for rotators and non-rotators with the p-value $= 1.2 \times 10^{-5}$, and for rotators and the control sample (p-value $= 5 \times 10^{-3}$). At the same time the distribution of swing amplitudes in the non-rotators and control sample sources is indistinguishable according to the test (p-value $= 0.35$). The maximum difference between the CDFs of non-rotators and rotators is 0.29. It is reached at $\Delta\theta_{\max} \approx 25°$. Even if we exclude the 14 rotations (i.e. the largest $\Delta\theta_{\max}$ swings) of the main sample blazars, rotators still remain different from the non-rotators (p-value $= 2 \times 10^{-3}$).

A similar analysis (as the one for $\Delta\theta_{\max}$) for the distributions of EVPA swing rates leads to the same conclusion. The null-hypothesis is rejected for the rotators and the non-rotators (p-value $= 1.4 \times 10^{-6}$) and rotators vs. the control sample (p-value $= 5 \times 10^{-3}$), while it can not be rejected for the non-rotators and control sample (p-value $= 0.18$).

We therefore conclude that blazars with detected rotations show significantly larger $\Delta\theta_{\max}$ and faster EVPA variations when compared to blazars with no detected rotations. This difference cannot be attributed to differences in the sampling properties of the data sets. Therefore, the lack of detection of EVPA rotations in the "non-rotators" member of the main sample, as well as the blazar in the control sample, may have a physical origin. Most of the non-rotators in the main and control samples may never show an EVPA rotation.

4 RANDOM WALKS AS THE ORIGIN OF EVPA ROTATIONS

4.1 MC simulations of EVPA swings

Potentially EVPA swings can be explained by a stochastic process, which is physically justified by a presence of many independent cells in the emission region (e.g. Jones et al. 1985; D'Arcangelo et al. 2007). According to this interpretation, the magnetic field is turbulent and apparent rotations result from a random walk of the full polarization vector direction as new cells with random magnetic field orientations appear in the emission region (Marscher 2014). In order to estimate the probabilities that the EVPA rotations we observed with RoboPol are produced by this kind of multicell random walk process we performed MC simulations of the stochastic variability of the polarization vector on the QU plane following Kiehlmann et al. (2013).

For each blazar where an EVPA rotation event was observed, we created 10^4 artificial light curves, each one with duration T_{obs}. The time steps Δt_{i} between consecutive points were drawn from a truncated power-law distribution, which approximates well the distribution of the time steps in all observed lightcurves. The parameters of this distribution ($\Delta t_{\min}$, $\Delta t_{\max}$ and the power-law index) were determined by fitting it to the distribution of observed Δt_{i} for each object.

The total flux density I_{i} emitted at each time step Δt_{i}, was drawn from a log-normal distribution. Such a distribution approximates reasonably well the distribution of the observed flux densities for all blazars. The mean and variance of the log-normal distribution was set equal to the sample mean and variance of the distribution of the flux density of each blazar.

The maximum possible fractional polarization produced by a uniform magnetic field is $P_{\max} = (\alpha + 1)/(\alpha + 5/3) \approx$
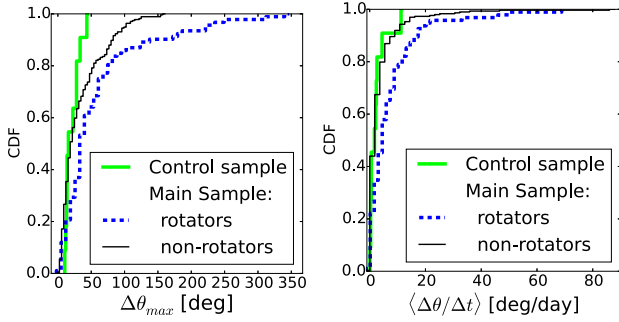
Figure 4. CDFs of $\Delta\theta_{\max}$ and average rates for the main sample rotators (95 EVPA swings), the main sample non-rotators (298 swings) and control sample sources (11 swings). See Sec. 3.4 for details.

0.78 (Pacholczyk 1970). In the case of unresolved emission region comprising N independent cells with a uniform magnetic field, but randomly oriented among them, the average fractional polarization is given by the equation (Hughes & Miller 1991):

$$\langle P_{\mathrm{obs}}\rangle \approx \frac{P_{\max}}{\sqrt{N}}. \tag{1}$$

We used this equation and the observed average polarization fraction, $\langle P_{\mathrm{obs}}\rangle$, to estimate the number of cells, N, for each blazar. Each k-th cell at i-th time step was assigned a flux density $I_{i,k}$ (which was set equal to I_i/N for all cells at each time step) and a set of fractional Stokes parameters $q_{i,k}$ and $u_{i,k}$. They were found as

$$\begin{cases} q_{i,k} = q_{i,k}^0 \frac{P_{\max}}{\sqrt{(q_{i,k}^0)^2 + (u_{i,k}^0)^2}} \\ u_{i,k} = u_{i,k}^0 \frac{P_{\max}}{\sqrt{(q_{i,k}^0)^2 + (u_{i,k}^0)^2}}, \end{cases} \tag{2}$$

where $q_{i,k}^0$ and $u_{i,k}^0$ are two numbers drawn from the standard normal distribution. Thereby the emission of each cell has polarization fraction $P_{\max}$. The sums $Q_i = I_i \sum_{k=1}^{N} q_{i,k}$ and $U_i = I_i \sum_{k=1}^{N} u_{i,k}$ determine the total Stokes parameters of the emitting region at each time step.

At each time step the Stokes parameters of $N_{\mathrm{var}}(\Delta t_i)$ cells, selected randomly, were replaced by new values. The number of cells for replacement was estimated (from the average variance of the polarization degree) as follows:

$$N_{\mathrm{var}}(\Delta t_i) = \frac{\Delta t_i}{\langle \Delta t\rangle} \frac{\sigma(P_{\mathrm{obs}})}{\langle P_{\mathrm{obs}}\rangle} N, \tag{3}$$

where $\sigma(P_{\mathrm{obs}})$ is the observed standard deviation of the degree of polarization for each blazar, and $\langle \Delta t\rangle$ is the average time difference between observations.

It was confirmed that the simulated and observational data in corresponding blazars have similar statistical properties. Namely, the standard deviation and average of the polarization fraction are consistent with $\sigma(P_{\mathrm{obs}})$ and $\langle P_{\mathrm{obs}}\rangle$.

4.1.1 Individual rotations

Using the algorithm described in Sec. 3, i.e. the same algorithm we used to identify rotations in real data, we identified all rotations in the simulated data and found the number N_{rot} of "successful" data sets, where at least one

Table 5. Random walk modelling results for EVPA rotations detected by RoboPol in 2013. (1) - blazar identifier; (2) - occurrence of rotations with $\Delta\theta_{\mathrm{max,simul}} \geq \Delta\theta_{\mathrm{max,obs}}$ estimated from the simulations; (3) - probability that a rotation produced by the random walk will be observed in T_{obs}.

| Blazar ID	T_{occ} (d)	P(RW)
RBPLJ0136+4751	505	0.11
RBPLJ0259+0747	151	0.48
RBPLJ0721+7120	325	0.28
RBPLJ0854+2006	142	0.36
RBPLJ1048+7143	180	0.79
RBPLJ1555+1111	128	1.00
RBPLJ1558+5625	266	0.51
RBPLJ1806+6949	965	0.15
RBPLJ1806+6949	259	0.55
RBPLJ1927+6117	137	0.98
RBPLJ2202+4216	633	0.21
RBPLJ2232+1143	1557	0.09
RBPLJ2232+1143	178	0.87
RBPLJ2243+2021	183	0.92
RBPLJ2253+1608	184	0.86
RBPLJ2311+3425	61	0.74

rotation with $\Delta\theta_{\max}$ larger or equal to $\Delta\theta_{\mathrm{max,obs}}$ was detected. We then estimated two ratios: $P(\mathrm{RW}) = \mathrm{N_{rot}}/10^4$ and $T_{\mathrm{occ}} = 10^4 \cdot T_{\mathrm{obs}}/\mathrm{N_{rot}}$. The first ratio determines the probability to observe an EVPA rotation due to a random walk for each one of the observed EVPA curves for the given T_{obs}. The second ratio determines the average time interval between random walk rotations (i.e. the average occurrence rate for each blazar). The probabilities $P(\mathrm{RW})$ and T_{occ} are listed in Table 5. The probabilities are larger than 10% in all but one object, and in some cases, they approach unity. This result indicates that the rotations we observed in some objects could be the result of a random walk process.

4.1.2 Rotations as a population

In this section we test the hypothesis that *all* the rotations observed by RoboPol in blazars of the main sample are produced by the stochastic process. According to the analysis in Sec. 3.4 blazars exhibiting rotations have different properties when compared to non-rotators. Therefore the sample of rotators must be considered separately.

We performed the following simulation. At each iteration, an artificial EVPA curve was generated individually for each rotator from the main sample as explained in Sec. 4.1. In each of the simuated EVPA curves we identified the largest rotation and constructed the CDF of $\Delta\theta_{\mathrm{max,simul}}$ among the blazars. An iteration was considered to be "successful" only in the case when the CDF of $\Delta\theta_{\mathrm{max,simul}}$ was lower or equal to the CDF of $\Delta\theta_{\mathrm{max,obs}}$, i.e. the simulated set of EVPA curves had higher or equal fraction of rotations of a given length compared to the observed set. In the cases of RBPLJ1806+6949 and RBPLJ2232+1143 where double rotations were observed, we simulated only the largest $\Delta\theta_{\max}$ rotations.

The CDF of $\Delta\theta_{\mathrm{max,obs}}$ along with a subset of 100 simulated CDFs is shown in Fig. 5. It was found that only 1.5% in 10^4 trials were "successful". Therefore, the probability that
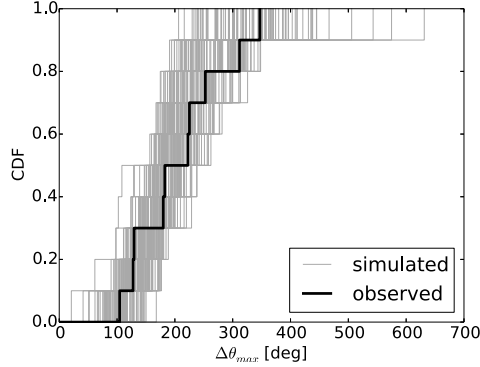
Figure 5. CDFs of $\Delta\theta_{\max}$ in observed and a subset of 100 simulated rotations.

10 largest rotations in blazars of the main sample observed in our monitoring campaign *all together* were produced by a random walk is $\sim 1.5\%$. If we repeat this simulation for the whole set of 16 EVPA rotations this probability is reduced to 0.5%.

We conclude that, although some of the rotation events that we have detected may have been caused by a random walk process (as it is modelled in this paper), this hypothesis is not a likely explanation of the total number of detected EVPA rotations in our data set.

5 OPTICAL EVPA ROTATIONS AND GAMMA-RAY ACTIVITY

5.1 Average gamma-ray flux during EVPA rotations

It has been suggested (e.g. Abdo et al. 2010a; Marscher et al. 2010) that rotations of EVPA in optical emission of blazars are physically related to gamma-ray flares.

In order to quantify a possible connection between EVPA rotations and gamma-ray activity, we first compared the average gamma-ray photon fluxes for each blazar during rotation events with the rest of the RoboPol season where no rotation was detected. Fig. 6 shows the gamma-ray lightcurves of blazars with detected rotations of EVPA. The green (light) area indicates the first year RoboPol observational season for each object and the pink (dark) area indicates the period of the detected rotation. The average photon fluxes (listed in Table 6) were calculated using the time intervals corresponding to the rotating and non-rotating periods as single time bins (or averaging fluxes for two/three non-rotating time bins in cases, where they are split by the rotations). The gamma-ray photon flux during a rotation was higher than the flux during the rest of the season at 1-σ level only in four cases. The average difference between the photon flux during rotations and along the rest of the season is $-0.3 \pm 3.4 \times 10^{-9}\,\mathrm{ph\,cm^{-2}\,s^{-1}}$. Thus, we do not observe any significant systematic change of the average gamma-ray photon flux simultaneous with the EVPA rotations.

However, a comparison of the mean flux levels during the rotation and over a relatively long period may not be the best way to search for a correlation between the gamma-ray

Table 6. Gamma-ray photon flux level during rotations and throughout the rest of the RoboPol season.

Blazar ID	Photon flux ($E > 100$ MeV) ($10^{-7}\mathrm{ph\,cm^{-2}s^{-1}}$)	
	rotation	no rotation
RBPLJ0136+4751	0.40 ± 0.14	0.59 ± 0.16
RBPLJ0259+0747	1.27 ± 0.21	< 0.71
RBPLJ0721+7120	0.95 ± 0.18	0.84 ± 0.11
RBPLJ0854+2006	0.33 ± 0.16	0.91 ± 0.18
RBPLJ1048+7143	3.39 ± 0.32	2.12 ± 0.11
RBPLJ1555+1111	0.51 ± 0.11	0.54 ± 0.05
RBPLJ1558+5625	< 0.34	0.21 ± 0.05
RBPLJ1806+6949	0.35 ± 0.15	0.40 ± 0.07
RBPLJ1806+6949	< 0.83	0.40 ± 0.07
RBPLJ1927+6117	0.29 ± 0.13	0.09 ± 0.05
RBPLJ2202+4216	4.67 ± 0.93	3.29 ± 0.21
RBPLJ2232+1143	3.82 ± 0.32	3.34 ± 0.25
RBPLJ2232+1143	4.55 ± 0.70	3.34 ± 0.25
RBPLJ2243+2021	0.11 ± 0.06	0.17 ± 0.04
RBPLJ2253+1608	6.98 ± 0.68	8.82 ± 0.19
RBPLJ2311+3425	2.09 ± 0.27	2.13 ± 0.35

activity and EVPA rotations. For instance in the cases of RBPLJ0721+7120 and first rotation of RBPLJ2232+1143, rotations are clearly coincident with prominent flares, although the average gamma-ray photon fluxes are indistinguishable, since the season comprises a number of flaring events with similar amplitude. Moreover, rotations of EVPA can either precede or follow gamma-ray flares according to various theoretical scenarios. It is therefore important to search for a possible correlation between EVPA rotations and gamma-ray flares.

5.2 Time lags between flares and EVPA rotations

In order to investigate this relation, we first identified all flares that happened in the gamma-ray light curves during the RoboPol observing season.

We adopted a formal definition of a gamma-ray flare similar to the one proposed by Nalewajko (2013): "a flare is a contiguous period of time, associated with a given photon flux peak, during which the photon flux exceeds half of the peak value, and this lower limit is attained exactly twice – at the start and at the end of the flare". However the definition was slightly changed because Nalewajko (2013) analysed a sample of the brightest flares ever detected by *Fermi* LAT, while we are interested in even smaller amplitude events. We found that a peak photon flux excess factor equal to 2/3, instead of the original 1/2 proposed by Nalewajko (2013), gives a better agreement with a visual identification of flares in the photon flux curves. Intervals of the photon flux curves identified as flares are marked by red (light) points in Fig. 6.

We searched for the closest gamma-ray flare to the rotation event of each rotator, and we fitted it using a profile with an exponential rise and decay. This kind of profile is commonly used for fitting an individual blazar flare pulse in optical, gamma and radio bands (e.g. Abdo et al. 2010b; Chatterjee et al. 2012):

$$F(t) = F_{\mathrm{c}} + F_{\mathrm{p}} \left(e^{\frac{t_{\mathrm{p}} - t}{T^{\mathrm{r}}}} + e^{\frac{t - t_{\mathrm{p}}}{T^{\mathrm{d}}}} \right)^{-1}, \qquad (4)$$
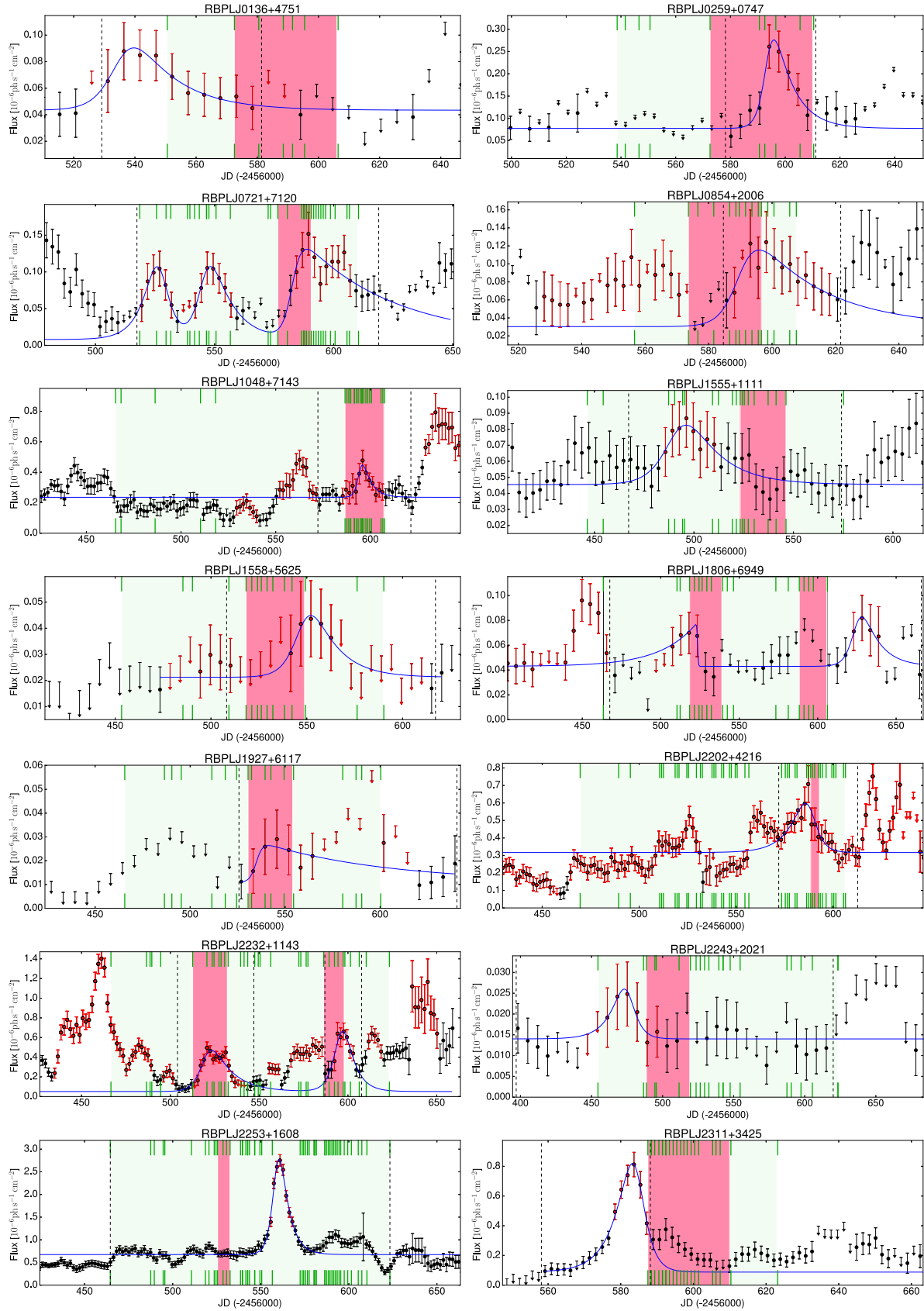
Figure 6. Gamma-ray light curves of objects with detected rotations of EVPA. The RoboPol observational season is marked by the green (light) area. The pink (dark) area shows duration of the rotation. Green ticks mark moments of our optical EVPA measurements. All curves are centred to the mean day of the RoboPol observing season. Detected flares are marked by red points, while the blue curve is the analytical function fit of the flares closest to observed rotations (see text for details). Vertical dashed lines indicate intervals of the light curves used in the fitting procedure.
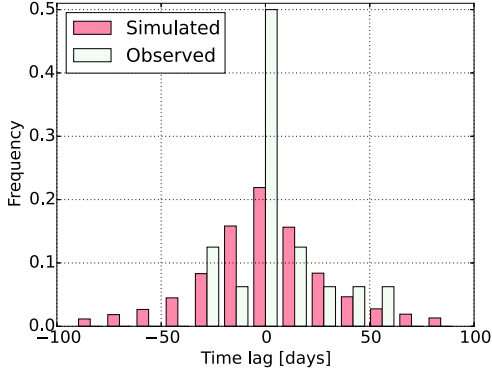
Figure 7. Distributions of observed τ_{obs} and simulated τ_{simul} time lags between middle points of rotations and t_{p} of gamma-ray flares.

Table 7. Gamma-ray flares fitting results. (1) - blazar identifier; (2) - time difference, τ_{obs}, between t_{p} of the closest gamma-ray flare and middle point of the rotation (positive means leading flare); (3) - gamma-ray flare amplitude measured relative to the average photon flux of the blazar from 2FGL.

Blazar ID	τ_{obs} (d)	γ-flare rel. ampl.
RBPLJ0136+4751	53.8	0.6 ± 0.08
RBPLJ0259+0747	-2.4	15.1 ± 2.9
RBPLJ0721+7120	0.8	1.0 ± 0.5
RBPLJ0854+2006	-5.3	2.5 ± 1.1
RBPLJ1048+7143	2.5	7.3 ± 3.6
RBPLJ1555+1111	42.9	1.1 ± 0.2
RBPLJ1558+5625	-14.8	1.9 ± 0.9
RBPLJ1806+6949	5.4	0.7 ± 0.6
RBPLJ1806+6949	-27.8	1.3 ± 0.4
RBPLJ1927+6117	7.5	0.6 ± 0.2
RBPLJ2202+4216	3.1	3.1 ± 0.6
RBPLJ2232+1143	2.6	7.3 ± 1.5
RBPLJ2232+1143	-3.7	12.1 ± 1.5
RBPLJ2243+2021	29.0	0.7 ± 0.4
RBPLJ2253+1608	-30.2	1.7 ± 0.2
RBPLJ2311+3425	18.8	16.6 ± 1.3

where F_{c} represents an assumed constant level underlying the flare, F_{p} measures the amplitude of the flare, t_{p} describes the time of the peak (it corresponds to the actual maximum only for symmetric flares), T^{r} and T^{d} measure the rise and decay time, respectively. All the parameters were set to be free, while initial values used in the fitting procedure were estimated from the photon flux curves. Upper limits of the light curve were not used in the fitting procedure. In the case of RBPLJ0721+7120 three flares that occurred during the observing season were fitted simultaneously because a single flare fit resulted in an unrealistic F_{c} value. In the cases of double rotations in RBPLJ1806+6949 and RB-PLJ2232+1143 the flares closest to the rotations were also fitted together to provide a consistent F_{c} value. In addition, in three cases, the closest flares happened just outside the RoboPol season interval. The best fitting curves are shown in Fig. 6.

We estimated time lags, τ_{obs}, between rotations and the closest gamma-ray flares as $\tau_{\mathrm{obs}} = \overline{T^{\mathrm{rot}}} - t_{\mathrm{p}}$, where $\overline{T^{\mathrm{rot}}}$ is the middle point of each EVPA rotation, defined as $t_{\mathrm{rot,start}} + \frac{T_{\mathrm{rot}}}{2}$ (see Table 7). The time lags have a distribution, shown by green (light) bars in Fig. 7, with mean and standard deviation equal to 5.1 and 21.8 d, respectively. The distribution is indistinguishable from the normal distribution $N(0, 21.8)$ following the K-S test (p-value = 0.39). Thereby *we do not find any preference for positive or negative* τ_{obs}. A distribution of observed time lags is expected to be close to a normal distribution with the mean at zero if rotations of the EVPA are not connected to gamma-ray flares. Because, in this case, the overall distribution is produced by a set of random values each having distributions of different widths and symmetric with respect to zero. For this reason the time lags distribution does not, on its own, support a physical connection between gamma-ray flares and rotations. However theoretical models allow for either positive or negative lags, depending on conditions and emission region properties, when a physical connection between rotations and gamma-ray flares does exist (Zhang et al. 2014). Therefore, a physical connection cannot be excluded based on the distribution of τ_{obs}.

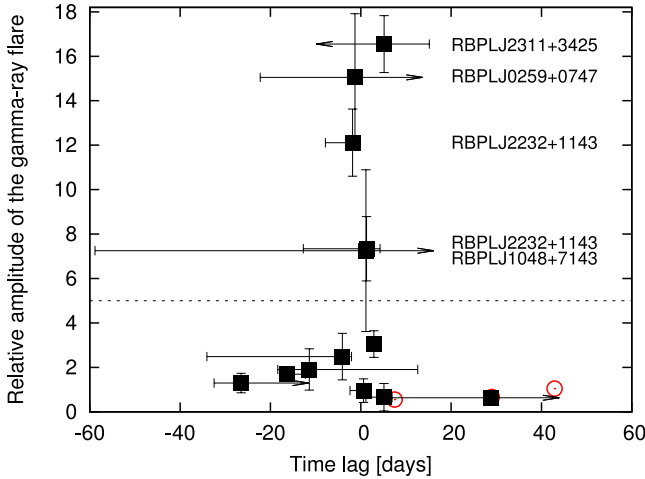### 5.3 Relation of gamma-ray flare amplitudes and time delays

We normalized the amplitude, F_{p}, of the gamma-ray flare closest to the EVPA rotation event by the average photon flux of each blazar (as listed in 2FGL; Nolan et al. 2012). Corresponding values are listed in Table 7 and plotted as a function of τ_{obs} in Fig. 8. The filled black squares show redshift-corrected time lags, i.e. $\tau_{\mathrm{corr}} = \tau_{\mathrm{obs}}/(1 + z)$, while open circles show τ_{obs} for blazars with unknown z. The "errors" on the time lags are defined as fitting errors of t_{p} plus the time difference between the first/last point of a rotation event, and the previous/next closest point of the EVPA curve. Due to the lack of data in some cases these "uncertainties" are undefined, while in others, due to sparse sampling, they are almost certainly overestimated.

A noticeable feature is that τ_{corr} is in the range $(-6, +6)$ d for the most prominent gamma-ray flares. Basically, all five brightest flares have happened almost simultaneously with EVPA rotation events. The brightest flare which has the largest deviation from the zero-delay is the flare of RB-PLJ2311+3425 where the start point of the rotation is undefined and therefore the time-delay has a large uncertainty.

There are three more flares with similarly small time lags, and small relative amplitudes. Thus a small separation between a flare and a rotation is not a sufficient condition for extraordinary brightness of the high-energy flare.

Separating the flares into two subsamples of high and low amplitude events (dashed line in Fig. 8) we examined the significance of the difference in time delays between them. The mean of the absolute τ_{obs} values for the high and low amplitude subsamples is 5.2 and 20.1 d, respectively. According to the Student's t-test (e.g. Wall & Jenkins 2012), the difference between the two mean values is somewhat significant (p-value = 0.025).

Figure 8. Time lags, $\tau_{\rm obs}$, versus normalized gamma-ray flare amplitude, $F_{\rm p}$. Redshift corrected and non-corrected $\tau_{\rm obs}$ values are plotted with filled squares and open circles, respectively.

5.4 Accidental proximity of rotations and gamma-ray flares

5.4.1 Individual blazars

In order to estimate the probability of the accidental observed proximity in time of rotations and gamma-ray flares, we performed MC simulations using the observed gamma-ray photon flux curves. This allows us to account for the real variability of blazars in the gamma-ray band. For each rotator we processed a long-term set of *Fermi* LAT data ($54683 \le {\rm MJD} \le 57065$) with time bins equal to the ones used in Sec. 5.2. Then we identified and fitted all gamma-ray flares following the procedure described previously, using the same photon flux excess factor of 1.5. The number of flares identified in the photon flux curves of rotators is in the range of 12 - 76. After that we randomly assigned the middle point of a simulated rotation to a time on the photon flux curve and measured the time lag between the rotation and the closest gamma-ray flare, $\tau_{\rm simul}$. Repeating this simulation 10^4 times for each blazar, we determined the distributions of time delays $\tau_{\rm simul}$. Using these distributions, we estimated the probability of $\tau_{\rm obs}$ to be produced by chance $P(\tau_{\rm obs})$, by calculating the fraction of simulations where $\tau_{\rm simul} \le \tau_{\rm obs}$. The probabilities range between 3 and 78 per cent (see Table 8). Pink (dark) boxes in Fig. 7 indicate the distribution of $\tau_{\rm simul}$, using the results from the simulation for all blazars. According to the K-S test the null hypothesis that $\tau_{\rm simul}$ and $\tau_{\rm obs}$ are drawn from the same distribution can not be rejected (*p*-value = 0.38). Therefore, it is possible that the $\tau_{\rm obs}$ values we observed, may be accidental for each of the blazars in the sample.

In Sect. 4.1 we determined the probability of the EVPA rotations to be observed in our observing window assuming that they are produced by a stochastic process. The simulations described above give us the probability of an accidental simultaneity between these rotations and gamma-flares. Therefore the probability of superposition of both independent events: (a) random rotation *and* (b) random proximity to a gamma-ray flare, can be estimated as a product of the

Table 8. Modelling results for the connection between EVPA rotations detected by RoboPol in 2013 and gamma-ray flares. (1) - blazar identifier; (2) probability of an accidental time lag; (3) - combined probability of a rotation being produced by the random walk and located as close to the corresponding gamma-ray flare as it was observed.

Blazar ID	$P(\tau_{\rm obs})$	$P({\rm RW} + \tau_{\rm obs})$
RBPLJ0136+4751	0.75	0.08
RBPLJ0259+0747	0.03	0.02
RBPLJ0721+7120	0.04	0.01
RBPLJ0854+2006	0.23	0.08
RBPLJ1048+7143	0.14	0.11
RBPLJ1555+1111	0.72	0.72
RBPLJ1558+5625	0.20	0.10
RBPLJ1806+6949	0.10	0.02
RBPLJ1806+6949	0.49	0.27
RBPLJ1927+6117	0.08	0.08
RBPLJ2202+4216	0.21	0.04
RBPLJ2232+1143	0.14	0.01
RBPLJ2232+1143	0.19	0.17
RBPLJ2243+2021	0.48	0.44
RBPLJ2253+1608	0.78	0.67
RBPLJ2311+3425	0.56	0.41

respective probabilities. These combined probabilities are less than 5 per cent for five events (see column 3 of Table 8). This result indicates that, at least for some rotations, the random walk model *and* the absence of any physical connection between the EVPA variability and high-energy activity is an unfavourable interpretation.

5.4.2 Rotators as a population

In order to assess the probability that the *entire set* of the time lags appeared in the main sample rotators in a random way, we run the following simulation. Repeating the procedure described in Sec. 5.2 we identified and fitted all flares in the gamma-ray photon flux curve ($54683 \le {\rm MJD} \le 57065$) of each blazar from the main sample with a detected rotation. Then placing a simulated rotation at a random position on each of the gamma-ray curves, we defined the shortest time lag between the central point of the rotation and $t_{\rm p}$ of the nearest flare. After this the CDF of absolute values of the simulated time lags was constructed for the set of 14 events.

Repeating the routine 10^6 times we found that only one out of every 5000 simulations produces a CDF which is in its entirety located closer to zero or coincides with the CDF of observed time lags (see Fig.9). Thereby we estimate the probability that all 14 delays together were produced by chance as 2×10^{-4}. When we repeat this procedure for all 16 rotations together including two non-main sample events, the estimated probability decreases to 5×10^{-5}. Therefore, it is very unlikely that none of the observed EVPA rotations is related physically to the flaring activity in gamma-rays.
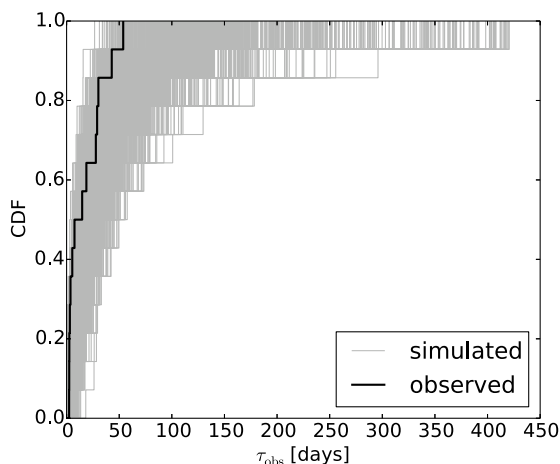
Figure 9. CDFs of the time lags between the EVPA rotations middle points and t_p of the closest gamma-ray flares for the main sample rotators. Black line – observed time lags, thin grey lines - 10^4 simulated values for the whole sample of rotations (see text for details).

6 CONCLUSIONS

During the first season of operation of the RoboPol project, we detected 16 rotations of the polarization plane in optical emission of blazars. These detections double the existing list of such events. All EVPA rotations are observed in blazars which are detected by *Fermi*, in agreement with previous experiments, which have detected similar events in the same class of objects. Our strategy of monitoring both gamma-ray–loud and quiet samples, suggests that the lack of EVPA rotations detection by RoboPol in gamma-ray–quiet objects cannot be due to a difference in the sampling pattern. Combining our results with those reported in the literature we found that rotations can be detected in both TeV and non-TeV emitters. Our results also indicate that all subclasses of blazars show rotations of the EVPA (regardless of the position of the synchrotron peak maximum or the BL Lac/FSRQ dichotomy). We expect that the results after the 3-yr planned RoboPol monitoring campaign will allow an accurate determination of the rotations rate in the various blazar subclasses.

Analysis of the first-year data shows that blazars with detected rotations have significantly faster and longer EVPA swings when compared to non-rotators. This suggests that rotations of EVPA may be specific for a particular activity state or for a subclass of blazars with peculiar properties.

The fact that EVPA rotations have been detected only in gamma-ray–loud objects already suggests a physical relation between gamma-ray and optical polarization variability in blazars. Nevertheless, we used extensive MC simulations to investigate whether the EVPA rotations we observed can be produced by a random walk process of the polarization vector. We found that a random walk process can result in EVPA rotations with $\Delta\theta_{\mathrm{max,simul}}$ as large as $\Delta\theta_{\mathrm{max,obs}}$ for the given Δt-median and T_{obs} of the individual RoboPol data sets. However, we also found that it is unlikely (probability is $\leq 1.5\times10^{-2}$), that *all* the rotations that we observed in the first RoboPol season are due to a random walk process.

The average gamma-ray photon fluxes do not show any significant systematic increase during the rotation events. We also found that, the time lags between rotations of the EVPA and nearest gamma-ray flares follow a Gaussian distribution with a mean $\sim$ zero.

We performed a second set of MC simulations in order to assess the randomness of the observed time delays. Our results suggest that, on an individual basis, the time lags we observe do not necessarily suggest a physical link between EVPA rotations and gamma-ray flares. On the other hand, when we consider the rotators as a population, it is highly unlikely ($p = 2\times10^{-4}$) that the proximity of EVPA rotations to gamma-ray flares is accidental in *all* cases. Therefore at least some EVPA rotations must be physically connected to the high-energy activity.

Our data suggest that, the highest amplitude gamma-ray flares may be physically connected with EVPA rotations, based on the fact that they are associated with smaller-than-average time lags. Perhaps there are two different types of gamma-ray flares, produced by different physical mechanisms. One of them may result in higher (than average) amplitude flares *and* EVPA rotation events. The other one may produce the rest of the smaller amplitude flares, which are not related with the remaining rotations, probably produced by a random walk process.

For the first time we studied a set of EVPA rotations discovered in a large, well-defined, regularly monitored sample of blazars. The diversity of results found in individual and population analysis shows the importance of these kinds of studies. The RoboPol monitoring of blazars will continue for at least two more years. The question about the mechanisms responsible for the EVPA rotations in blazars and their possible connection to the high-energy activity will be explored in more detail after accumulation of a larger data set by RoboPol.

The statistical analysis of our data set required us to make subjective choices regarding the details of our event definitions and the test statistics we used. These, for example, include the definition of a rotation, the definition of a "gamma-ray activity" (increase in gamma-ray flux during a rotation versus proximity to a gamma-ray flare peak), the definition and fitting procedure of a gamma-ray flare, use of the $\Delta\theta_{\mathrm{max}}$ and $|\tau_{\mathrm{obs}}|$ CDFs as test statistics and so forth. Making these choices introduces unavoidable and unquantifiable biases in our final results. However, our exploratory analysis of the first-year data presented here has allowed us to identify well-defined statistical questions, which we can address in a robust, a priori fashion using our second- and third-year data.

REFERENCES

Abdo A. A., et al., 2010a, Nature, 463, 919
Abdo A. A., et al., 2010b, ApJ, 722, 520
Acero F., Ackermann M., Ajello M., et al., 2015, ApJS, 218, 23
Ackermann M., et al., 2012, ApJS, 203, 4
Agudo I., et al., 2011, ApJL, 726, L13
Aleksić J., et al., 2014a, A&A, 567, A41
Aleksić J., et al., 2014b, A&A, 569, A46
Angel J. R. P., Stockman H. S., 1980, ARA&A, 18, 321
Atwood W. B., et al., 2009, ApJ, 697, 1071
Benítez E., Sorcia M., Hiriart D., 2013, in EPJ Web Conf. p. 7010
Bjornsson C.-I., 1982, ApJ, 260, 855
Blandford R. D., Levinson A., 1995, ApJ, 441, 79
Chatterjee R., et al., 2012, ApJ, 749, 191
D'Arcangelo F. D., et al., 2007, ApJL, 659, L107
Donato D., Ghisellini G., Tagliaferri G., Fossati G., 2001, A&A, 375, 739
Falco E. E., Kochanek C. S., Muñoz J. A., 1998, ApJ, 494, 47
Fan J. H., Yang J. H., Yuan Y. H., Wang J., Gao Y., 2012, ApJ, 761, 125
Ghisellini G., Tavecchio F., Foschini L., Ghirlanda G., 2011, MNRAS, 414, 2674
Healey S. E., et al., 2008, ApJS, 175, 97
Hewitt A., Burbidge G., 1987, ApJS, 63, 1
Hughes P. A., Miller L., 1991, Introduction: synchrotron and inverse-Compton radiation. p. 1
Ikejiri Y., et al., 2011, PASJ, 63, 639
Jones T. W., Rudnick L., Aller H. D., Aller M. F., Hodge P. E., Fiedler R. L., 1985, ApJ, 290, 627

Kiehlmann S., et al., 2013, in EPJ Web Conf.. p. 6003
Kikuchi S., Mikami Y., Inoue M., Tabara H., Kato T., 1988, A&A, 190, L8
King O. G., et al., 2014, MNRAS, 442, 1706
Kinman T. D., Lamla E., Wirtanen C. A., 1966, ApJ, 146, 964
Konigl A., Choudhuri A. R., 1985, ApJ, 289, 188
Larionov V. M., et al., 2008, A&A, 492, 389
Larionov V. M., Jorstad S. G., Marscher A. P., Morozova D. A., Troitsky I. S., Blinov D. A., Kopatskaya E. N., Larionova E. G., 2011, Fermi Symp. p.
Larionov V. M., et al., 2013a, in EPJ Web Conf.. p. 4019
Larionov V. M., et al., 2013b, ApJ, 768, 40
Marscher A. P., 2014, ApJ, 780, 87
Marscher A. P., et al., 2008, Nature, 452, 966
Marscher A. P., et al., 2010, ApJL, 710, L126
Monet D. G., et al., 2003, AJ, 125, 984
Moore R. L., et al., 1982, ApJ, 260, 415
Murphy D. W., Browne I. W. A., Perley R. A., 1993, MNRAS, 264, 298
Nalewajko K., 2013, MNRAS, 430, 1324
Nieppola E., Tornikoski M., Valtaoja E., 2006, A&A, 445, 441
Nilsson K., Pursimo T., Sillanpää A., Takalo L. O., Lindfors E., 2008, A&A, 487, L29
Nilsson K., Takalo L. O., Lehto H. J., Sillanpää A., 2010, A&A, 516, A60
Nolan P. L., et al., 2012, ApJS, 199, 31
Ofek E. O., et al., 2012, PASP, 124, 854
Pacholczyk A. G., 1970, Radio Astrophysics: Nonthermal Processes In Galactic And Extragalactic Sources. W.H. Freeman and Co., San Francisco, CA
Pavlidou V., et al., 2014, MNRAS, 442, 1693
Polatidis A. G., Wilkinson P. N., Xu W., Readhead A. C. S., Pearson T. J., Taylor G. B., Vermeulen R. C., 1995, ApJS, 98, 1
Poutanen J., Stern B., 2010, ApJL, 717, L118
Sasada M., et al., 2010, PASJ, 62, 645
Sasada M., et al., 2011, PASJ, 63, 489
Sasada M., et al., 2012, PASJ, 64, 58
Schlafly E. F., Finkbeiner D. P., 2011, ApJ, 737, 103
Serkowski K., Mathewson D. S., Ford V. L., 1975, ApJ, 196, 261
Sillanpää A., Takalo L. O., Nilsson K., Kikuchi S., 1993, Ap&SS, 206, 55
Tagliaferri G., et al., 2000, A&A, 354, 431
Uemura M., et al., 2010, PASJ, 62, 69
Vermeulen R. C., Ogle P. M., Tran H. D., Browne I. W. A., Cohen M. H., Readhead A. C. S., Taylor G. B., Goodrich R. W., 1995, ApJL, 452, L5
Wall J. V., Jenkins C. R., 2012, Practical statistics for astronomers. Cambridge University Press, Cambridge
Wills D., Wills B. J., 1976, ApJS, 31, 143
Zhang H., Chen X., Böttcher M., 2014, ApJ, 789, 66
de Grijp M. H. K., Keel W. C., Miley G. K., Goudfrooij P., Lub J., 1992, A&AS, 96, 389

This paper has been typeset from a T$_{\rm E}$X/L$^{\rm A}$T$_{\rm E}$X file prepared by the author.